2021 43rd Annual International Conference of the
IEEE Engineering in Medicine & Biology Society (EMBC)
Oct 31 - Nov 4, 2021. Virtual Conference

Increasing the Image Contrast via Fast Fluorescence Photobleaching

Radim Kolář, Larisa Chmelíková, Tomáš Vičar, Ivo Provazník

Abstract— **This paper focuses on the analysis of image sequences acquired during fast photobleaching using a standard wide-field microscope. We show that the photobleaching rate estimated for each pixel is not constant for the whole field of view, but it provides a new spatially variant parametric image related to the cell structure and diffusion of fluorophores. We also provide an alternative way to estimate a pixel-wise photobleaching rate with significantly less computation time than exponential model fitting.**

Clinical Relevance— **This method provides an additional way how fluorescence photobleaching might be used for increasing the image contrast**

I. Introduction

Fluorochromes are widely used in life-science microscopy to detect molecular expression by a specific antigen-antibody reaction. During the imaging process, photobleaching typically occurs. This phenomenon is defined as photo-induced chemical destruction of fluorophores stimulated by excitation light. The presence of oxygen in the sample and high excitation intensity are the two most contributing factors to photobleaching. This process is somewhat negative, and an effort to correct this effect on the acquired image can be found in research papers [1, 2]. However, it can also be utilized to study the local mobility of fluorescently labelled particles with *fluorescence recovery after photobleaching* (FRAP) methods [3]. These methods are widely used, and 2D/3D application has been presented in the last decades.

The emitted light intensity decrease due to photobleaching is typically mono- or bi-exponential with one or two photobleaching rate(s), respectively. The photobleaching rate depends on different parameters, including illumination intensity and local intracellular environment (e.g., local free oxygen concentration), but it also depends on the local fluctuation of free or conjugated fluorescence molecules. It has been shown [4] that pixel-wise fitting of a mono-exponential decay model provides spatially varying photobleaching rates that vary more than one order of magnitude inside the cell. Thus, the detail examination and visualization of the photobleaching rate might bring new information related to this phenomenon.

In this paper, we investigate the photobleaching rate based on the mono-exponential model, and we derive a fast approximation for its estimation in a pixel-by-pixel manner. We show that the spatial distribution of this parameter provides a higher image contrast in comparison to a single image frame or an average frame.

II. Method

A. Experimental protocol

Osteogenic sarcoma cell line (SAOS-2; ATCC, HTB-85) was cultured in high glucose Dulbecco's Modified Eagle Medium containing 1% L-glutamine, 10% Fetal Bovine Serum and 1% Penicillin-streptomycin (100 $U \cdot ml^{-1}$:100 $\mu g \cdot ml^{-1}$) and maintained at 37°C in a humidified atmosphere containing 5% CO_2. When the culture reached 80 to 100% confluence, then cells were split by applying 0.25% trypsin-EDTA solution. All chemicals used for cell culture were purchased from Sigma-Aldrich (St. Louis, MO, USA). For microscopy imaging, the cells were seeded on fibronectin-coated glass-bottom dishes with 35 mm diameter (Cellvis, Mountain View, CA, USA) at a density of $2 \cdot 10^4$ $cells \cdot cm^{-2}$. Experimental cell samples were stained with CellTracker™ Green CMFDA Dye (CMFDA; Invitrogen, Carlsbad, CA, USA) in a final concentration of 1 µM in serum-free medium for 15 minutes.

The image data was acquired with a fluorescence wide-field Nikon TS2-S-SM microscope equipped with E Plan objective 100x/1.25. The monochrome global shutter camera UI-3280CP-M-GL R2 camera (iDS Imaging GmbH., Germany) 2456 × 2054 pixels with uEye Cockpit software was used for acquisition. Short sequences with FITC filter cube (475/535 nm excitation/emission wavelength), lasting from 5 to 15 seconds, were recorded with framerate of 14 fps. The specific field of view was found in phase-contrast mode. Then, the microscope was switched to fluorescence mode with a preset intensity of excitation light, which was set beforehand. An example of several frames and the averaged image is shown in Fig. 1.

The confocal laser scanning microscope Leica TCS SP8 X (Leica Microsystems, Wetzlar, Germany) was used to capture high-resolution images of the same cells for subjective comparison. This microscope was equipped with a pulsed white light laser, and a hybrid detector was used for data acquisition. The excitation wavelength was set to 492 nm, and the detection range was set between 505 and 545 nm. The samples were observed using 100x oil immersion objective (Leica, HC PL APO 100x/1.44 Oil CORR CS). The microscopic images were obtained with a spatial resolution of 2048 × 2048 pixels, 116.25 × 116.25 µm physical length, bit

R. Kolář, L. Chmelíková, T. Vičar, I. Provazník is with the Brno University of Technology, Faculty of Electrical Engineering and Communication, Department of Biomedical Engineering, Brno, Czech Republic (corresponding author e-mail: kolarr@vut.cz).

depth of 16 bits, 100 Hz scan speed. An example of this image is shown in Fig. 3.

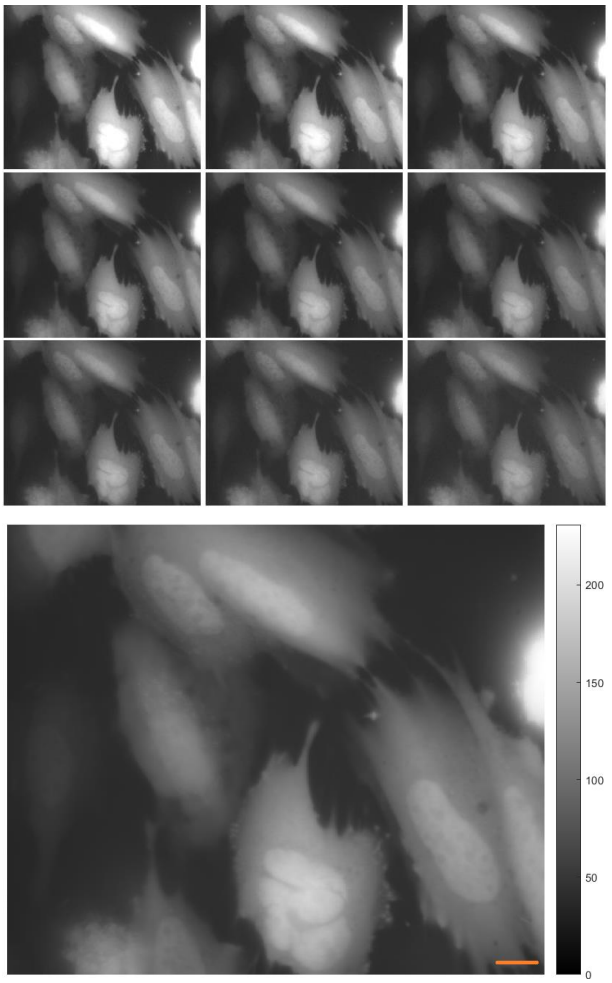

Fig. 1. Top: Nine frames of the recorded sequence acquired by the wide-field microscope show the decreasing emission intensity. Bottom: Average image of the sequence. The scale bar corresponds to 10 μm.

B. Photobleaching model

There are different types of photobleaching curves, which are described by negative exponential behavior. Mono- and bi-exponential models are the most accepted models, which describe the increase of the emission light intensity as a function of time considering the single or two-population model, respectively [2]:

$$I(t) = I_0 e^{-\frac{t}{\tau}} \qquad (1)$$

(1)

$$I(t) = I_0 e^{-\frac{t}{\tau_1}} + I_0 e^{-\frac{t}{\tau_2}} \qquad (2)$$

Here the constants τ, τ_1 and τ_2 represent the rate of photobleaching and I_0 represent the initial fluorescence intensity. These equations hold for every pixel. During the acquisition, the sampling in the spatial and time domain is performed. Thus we can write for the single exponential model:

$$I_0(x,y,n) = I_0(x,y).\, e^{-\frac{n.T}{\tau(x,y)}}, \qquad (3)$$

where the values $I_0(x,y)$ and $\tau(x,y)$ are spatially variant; T is the sampling period, and n is the time index. The τ value should be the same for the whole sample if the scene is static, i.e., without moving compartments and without a spatially variant environment, which affects the photobleaching. However, due to diffusion of the molecule and intracellular processes, its value will be spatial dependent, providing the $\tau(x,y)$ map. Furthermore, from an image processing point-of-view, it can provide a new parametric-based image contrast, as shown below.

C. Image data processing

Video-recording was further processed to estimate the parameters of the photobleaching models. This estimation was performed pixel-by-pixel after noise elimination by application of a spatial median filter with a 3x3 kernel. As a result, the spatial parametric maps for the mono-exponential model are created, i.e., $I_0(x,y)$ and $\tau(x,y)$) (see Fig. 2).

The *pixel-by-pixel* exponential fitting was performed in Matlab 2016b (MathWorks, Natic, USA) using the *fit* function with a monoexponential model and truth-region optimization. This approach is time-consuming because the number of fittings depends on the number of pixels on the chip of the camera, which is typically in the order of millions. In our case, the number is slightly over 5 million. As an alternative, a linear regression can be used to estimate the model parameters in a least-squares sense, exploiting a log transform, which will make the estimation faster. Nevertheless, the number of fitting curves is still very high. Therefore, we will describe an alternative approach to speed up the process. In our analysis, we focused on the variance of the photobleaching signal, and we relate this quantity to the parameters of the model.

Let's consider the *time* variance of the photobleaching signal:

$$\sigma(x,y)^2 = E\{I^2(x,y,n)\} - E\{I(x,y,n)\}^2. \qquad (4)$$

The expected value $E\{\cdot\}$ of the intensity signal can be estimated as a sum of samples of the exponential function divided by the number of samples, i.e.,

$$S(x,y) = \frac{1}{N} I_0(x,y) \sum_{n=0}^{N-1} e^{-\frac{nT}{\tau(x,y)}} \approx \frac{1}{N} \frac{I_0(x,y)}{1-e^{-\frac{T}{\tau(x,y)}}} \qquad (5)$$

The last expression is a sum of exponential sequence for an infinite number of samples, which can be considered in our case because the number of samples is in the order of hundreds.

The average value of the squared signal can be expressed similarly:

$$S_2(x,y) = \frac{1}{N} I_0^2(x,y) \sum_{n=0}^{N-1} e^{-\frac{2nT}{\tau(x,y)}} \approx \frac{1}{N} \frac{I_0^2(x,y)}{1-e^{-\frac{2T}{\tau(x,y)}}} \qquad (6)$$

The variance can be therefore written as:

$$\sigma^2 = \frac{1}{N} \frac{I_0^2}{1-e^{-\frac{2T}{\tau}}} - \left(\frac{1}{N} \frac{I_0}{1-e^{-\frac{T}{\tau}}} \right)^2 \qquad (7)$$

Here, we omitted the spatial coordinates for simplicity. We would like to obtain more straightforward expression relating the variance and τ. Thus, we apply Taylor expansion of the

exponential function ($exp(x) = 1 + x + \ldots$), which leads to simple expression, when considering only the linear term:

$$\sigma^2 = \frac{1}{N}\frac{I_0^2}{\frac{2T}{\tau}} - \frac{1}{N^2}\frac{I_0^2}{\left(\frac{T}{\tau}\right)^2} = \frac{I_0^2}{N}\frac{\tau}{T}\left(\frac{1}{2} - \frac{\tau}{NT}\right) \quad (8)$$

This leads to a quadratic equation relating to the variance and photobleaching rate, which has the following solution:

$$\tau_{1,2} = \frac{N \cdot T}{4}\left[1 \pm \sqrt{1 - 16\frac{\sigma^2}{I_0^2}}\right] \quad (9)$$

This solution is valid for positive discriminant, i.e., $I_0 > 4\sigma$, which is typically fulfilled for long acquisition. However, equation 8 can also be used for simpler τ estimation. For long acquisition, the second term in the bracket $\frac{\tau}{NT}$ of this equation can be neglected with respect to ½. This rough approximation provides a simple expression for the variance:

$$\sigma^2 \approx \frac{1}{2}\frac{I_0^2}{N}\frac{\tau}{T} \quad (10)$$

which leads to expression for τ estimation:

$$\tilde{\tau}(x,y) = 2NT\frac{\sigma^2(x,y)}{I_0^2(x,y)} \quad (11)$$

Thus, the photobleaching rate can be estimated for each pixel from the temporal variance and maximum value of the exponential decay. This expression is much easier to compute and significantly faster. Furthermore, we observed that it leads to high image contrast of the new parametric image $\tilde{\tau}(x,y)$.

III. Results

The presented approach was tested on sequences acquired according to the experimental protocol described in Section II A (see Fig. 1) and compared to high-resolution images acquired by a confocal microscope.

The parametric images showing the spatial distribution of $1/\tau(x,y)$ or $1/\tilde{\tau}(x,y)$, respectively are presented in Fig. 2. The inverse value of τ parameter is shown because it provides a similar intensity distribution as native images (the cells are brighter than the background). These images look quite similar with respect to the contrast of cells and intracellular compartments. The nuclei are more visible in the averaged fluorescence image (Fig. 2, top image), but the other cell structures have higher contrast in the parametric $\tilde{\tau}$-image; particularly the cell itself and some specific cell compartments (e.g. lysosomes, filopodia).

However, the values of the estimated photobleaching rates estimated by the proposed approach are almost three to five times larger in comparison with exponential fitting. This error is probably caused by the fact that the condition $\tau << NT$ is not fulfilled because the acquisition time was approximately five times higher than the photobleaching rate. However, we can clearly see higher image contrast, which enables to recognize detail intracellular structures.

Because the τ or $\tilde{\tau}$-image is noticeably more detailed than single frames or the averaged image, we also acquired the image data of the same cells (different field of view) with a confocal microscope. This image is shown in Fig. 3. Similar structures can be recognized in both images, particularly the high contrast filopodia and cell internal structures can be recognized in both confocal and $\tilde{\tau}$-image quite clearly.

Another example of $\tilde{\tau}$-image, acquired by the same experimental protocol is shown in Fig. 4 and Fig. 5, respectively.

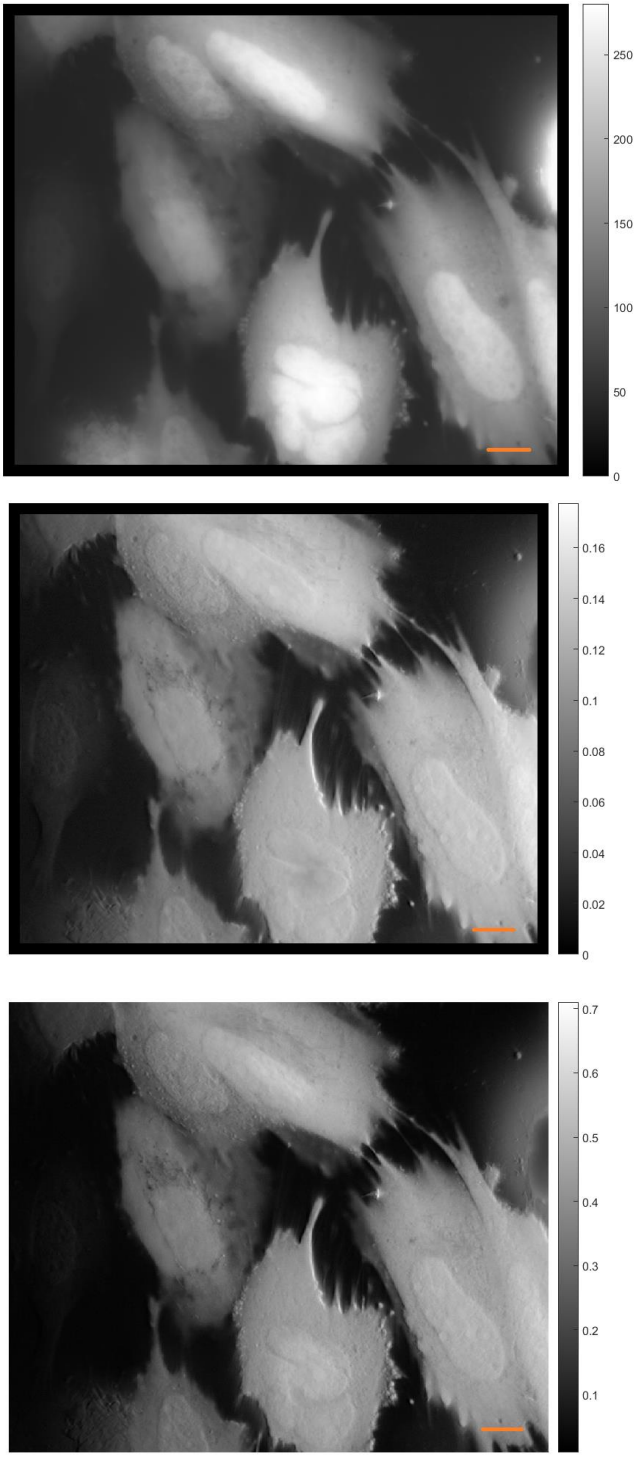

Fig. 2. Top: The spatial distribution of $I_0(x,y)$; Middle: Spatial distribution of $1/\tau(x,y)$ computed as fitting the exponential function to the intensity profile of each pixel; Bottom: Spatial distribution of $1/\tilde{\tau}(x,y)$ computed as the ratio of variance and $I_0(x,y)$ according to equation (11). The color bar represents $1/\tau$; the scale bar corresponds to 10 μm.

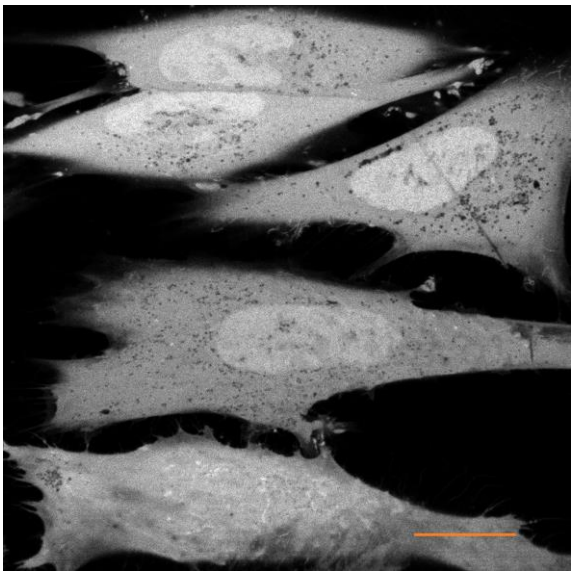

Fig. 3. The image of the same cells (SAOS-2), but the different field of view acquired by a confocal microscope. Scale bar represents 25 μm.

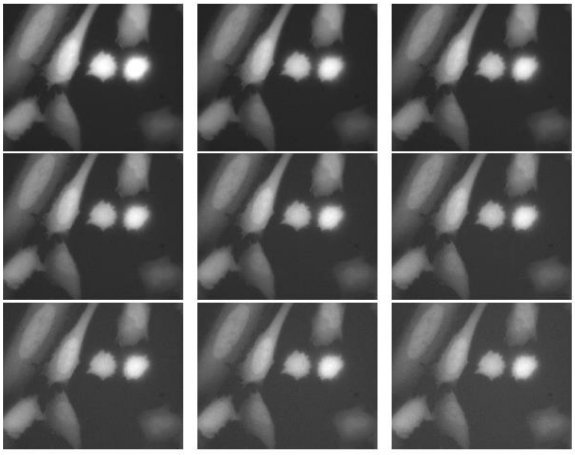

Fig. 4. Nine frames of another sequence (same cells, SAOS-2)

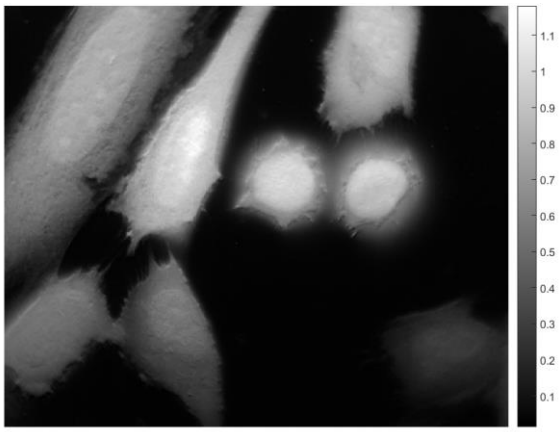

Fig. 5. Spatial distribution of $1/\tilde{\tau}(x,y)$ computed as the ratio of variance and $I_0(x,y)$ according to equation (11), computed from the second sequence shown in Fig. 4. The color bar represents 1/τ.

IV. Discussion and Conclusion

The proposed method showed that relative simple image sequence processing could bring interesting results in terms of new parametric image with better image contrast than a single frame or an average image. The theoretical resolution of used wide-field microscope with 100× objective is 229 nm, which provides sufficient resolution for imaging of the small compartments inside the cells, which are enhanced by the proposed approach.

The results will, of course, depend on the fluorescence dye. Here we used CellTracker™ Green CMFDA dye that conjugated with glutathione, located within the cell [5]. Thus, it allows visualization of the whole cell in contrast to a large number of fluorescent probes intended for visualization of the selected cell structure. Nevertheless, in our case, recognition of some structures at high magnification is also possible due to different concentrations of the dye in the organelles. The proposed method for image sequence analysis provides new parametric images with increased image contrast, which improves the recognition of the cell structure.

These first experiments open new possibilities for future research - application of different dyes and different setups, including various illumination intensities influencing the photobleaching rate.

Acknowledgment

This work has been supported by the Czech Science Foundation, grant number 18-24089S.

References

[1] J. A. Conchello, "Fluorescence photobleaching correction for expectation-maximization algorithm," Proceedings of SPIE 2412, Three-Dimensional Microscopy: Image Acquisition and Processing II, pp. 138-164, 1995

[2] N. B. Vicente, J. E. D. Zamboni, J. F. Adur, E. V. Paravani, V. H. Casco, "Photobleaching correction in fluorescence microscopy images", Journal of Physics: Conference Series, 90, 012068, 2007

[3] H. C. Ishikawa-Ankerhold, R. Ankerhold, Richard and G. P. C. Drummen, "Advanced Fluorescence Microscopy Techniques—FRAP, FLIP, FLAP, FRET and FLIM", Molecules, vol. 17, no. 4, pp. 4047-4132, 2012

[4] D. M. Benson, J. Bryan, A. L. Plant, A. M. Gotto Jr, L. C. Smith. "Digital imaging fluorescence microscopy: spatial heterogeneity of photobleaching rate constants in individual cells", Journal of Cell Biology, vol. 100, no. 4, pp.1309-1323, 1985

[5] J. Sebastia, R. Cristófol, M. Martín, E. Rodríguez-Farré, C. Sanfeliu, "Evaluation of fluorescent dyes for measuring intracellular glutathione content in primary cultures of human neurons and neuroblastoma SH-SY5Y", Cytometry Part A: The Journal of the International Society for Analytical Cytology, vol. 51, no. 1, pp. 16-25, 2003